View metadata, citation and similar papers at core.ac.uk

brought to you by CORE

provided by University of Strathclyde Institutional Repository

Strathprints Institutional Repository

Giuliese, G. and Palazzetti, R. and Moroni, F. and Zucchelli, A. and Pirondi, A. (2015) Cohesive zone modelling of delamination response of a composite laminate with interleaved nylon 6,6 nanofibres. Composites Part B: Engineering, 78. pp. 384-392. ISSN 1359-8368 , http://dx.doi.org/10.1016/j.compositesb.2015.03.087

This version is available at http://strathprints.strath.ac.uk/54011/

Strathprints is designed to allow users to access the research output of the University of Strathclyde. Unless otherwise explicitly stated on the manuscript, Copyright © and Moral Rights for the papers on this site are retained by the individual authors and/or other copyright owners. Please check the manuscript for details of any other licences that may have been applied. You may not engage in further distribution of the material for any profitmaking activities or any commercial gain. You may freely distribute both the url (http://strathprints.strath.ac.uk/) and the content of this paper for research or private study, educational, or not-for-profit purposes without prior permission or charge.

Any correspondence concerning this service should be sent to Strathprints administrator: strathprints@strath.ac.uk

COHESIVE ZONE MODELLING OF DELAMINATION RESPONSE OF A COMPOSITE LAMINATE WITH INTERLEAVED NYLON 6,6 NANOFIBERS

G. Giuliese[a], R. Palazzetti[b*], F. Moroni[c], A. Zucchelli[d], A. Pirondi[e]

[a]Industrial Engineering Department, University of Parma, viale G.P. Usberti 181/A, 43124 Parma, Italy (gregorio.giuliese@nemo.unipr.it, alessandro.pirondi@unipr.it).

[b]DMEM Department, University of Strathclyde, 75 Montrose Street, G1 1XJ Glasgow, UK (roberto.palazzetti@strath.ac.uk).

[c]Interdepartmental center SITEIA.PARMA, University of Parma, viale G.P. Usberti 181/A, 43124 Parma, Italy (moroni@ied.unipr.it).

[d]Department of Industrial Engineering, University of Bologna , viale del Risorgimento 2, 40134 Bologna, Italy (a.zucchelli@unibo.it).

* Principal Corresponding Author.

Abstract

This work simulates numerically Double Cantilever Beam and End Notched Flexure experiments on Carbon Fiber Epoxy Resin specimens that have been performed by some of the authors in a previous work. Specimens have been nanomodified by interleaving plies with a layer of electrospun nanofibers in the delaminated interface. Eight different configurations of nanofibers have been used as interleave, for a total of 9 configurations (8 nanomodified plus the virgin one) to be simulated for both kind of tests to identify the cohesive zone parameters corresponding to the effect of nanofiber diameter, nanolayer thickness and nanofiber orientation on the delamination behaviour of the composite.

Results showed that a bilinear damage law is necessary for almost all nanomodified configurations, and presented a clear relationship between nanomat layer parameters and the cohesive energy of the interface.

Keywords: *A. Polymer-matrix composites; A. Nanostructures; B. Delamination; C. Finite element analysis (FEA)*

1 Introduction

Composite laminates represent one of the most important technological developments of the last decades. They find application in a growing number of sectors and their importance is consequently increasing day by day. When a fracture takes place between two plies it takes the name of delamination, and is one of the most critical failure modes for laminates since it appears and grows without being visible from outside. A delaminated laminate can significantly loss stiffness and strength and still remains visibly unchanged. Many efforts were carried out in the last decades to mitigate delamination in composites, and a large number of researches can be found in literature, for instance, on testing [1-6] and modelling [7-15] delaminated materials.

It has been demonstrated that the delamination resistance of composite laminates could be significantly enhanced by means of layers of nanofibers laid down at ply interfaces [16-19]. Beside delamination resistance, nanointerleaved composite material showed an improvement on damping, flexural strength, and fatigue properties, [20].

Delamination of composite laminates interfaces is commonly simulated with cohesive zone model. These model, initially proposed by Dugdale [21] and Barrenblatt [22], describes the damage phenomena at the crack tip by means of a stress-opening relationship (cohesive law). Different shapes of the cohesive law have been defined in the literature for a better representation of the fracture phenomena: rigid linear cohesive laws are typically used for the brittle fracture [23], piece-wise linear cohesive laws and exponential cohesive laws are typically used for more ductile fracture [24, 25, 26]. Some works present cohesive zone models for the simulation of the failure behaviour of adhesively bonded joints [27, 28] Li et al. [29], dealing with the crack simulation of an adhesively bonded polymer-matrix composite material, noticed that the crack propagation was accompanied by a significant amount of fiber pull-out. In order to capture both the matrix cracking and the fiber pull out phenomena, they used a “bi-triangular” cohesive law. This was defined as the envelope of two cohesive laws: the first representing the matrix strength and the second representing the fiber bridging.

Turon et al. [30] studied the effects of the element size on the force/displacement response of a DCB test, showing that accurate simulations require elements length smaller than 1 mm, and a minimum number of 5 elements within the cohesive zone. They also showed that the interface stiffness can have a large influence on the accuracy of the solution.

This work presents a detailed finite element simulation analysis of composite laminates interleaved with nanofibers of different configuration.

Both triangular and bi-triangular laws are used in numerical analysis of Double Cantilever Beam (DCB) and End Notched Flexure (ENF) tests of virgin and nanomodified samples done in [18] on virgin and nanomodified Carbon Fiber Reinforced Plastic (CFRP) laminates with eight different configurations of nanofibers. Simulations using cohesive zone have a double purpose:

1) modelling the effect of the presence of a nanofibrous interleave into an epoxy-based composite laminate: the simulation has the purpose to link the geometrical feature of the nanofibrous mat to the global mechanical properties of the laminates;
2) providing a useful tool to designers who want to reinforce their laminates with nanofibers, in the perspective of using the cohesive zone parameters identified on DCB and ENF tests with different nanofibers in a process of virtual optimization of composite layup for a given application.

2. Experiments summary

The mode I (DCB) and mode II (ENF) fracture mechanic tests presented in [18] are briefly reported here. In the experiments, 20-plies specimens made of woven carbon fiber/epoxy resin were interleaved during the lay-up with a mat of Nylon 6,6 electrospun nanofibers between the 10^{th} and the 11^{th} ply, where delamination was forced to take part by placing a teflon insert at one side. Several nanofibrous mat configurations have been manufactured in order to investigate the effect of the nanofiber mat geometry on the behaviour of the laminate. In particular three geometrical features have been considered, and the same nomenclature used in [18] is being used here to identify the nanomodified configurations:

- nanofiber diameter of 150 and 500 nm, identified by the numbers 14 and 25, respectively;
- random and oriented nanofibers, identified by the letters “R” and “O”, respectively;
- nanomat thickness of 25 and 50 μm, identified by the letters “B” and “C” respectively.

Table 1 summarizes nanomodified configurations and the codes used throughout the paper.

3. Numerical modelling

The aim of the modelling is to identify a behavioural model based on cohesive zone to simulate the delamination in nanomodified interfaces from DCB and ENF tests. The simulations are performed with commercial code Abaqus with implicit time integration.

The traction-separation behaviour assigned to cohesive elements is the classical triangular law presented in Figure 1.

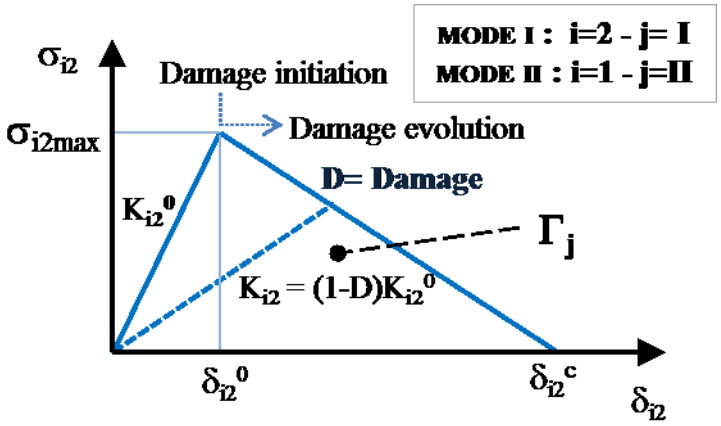

Figure 1.

Where σ represents the stress of the element, δ its opening and K its stiffness.

When a certain level of displacement (or stress) is reached, the stiffness and the strength are progressively reduced until the complete separation is obtained. This type of cohesive law fits reasonably well to a predominantly brittle fracture, for which the force/opening experimental curve presents an initial maximum peak followed by an exponential-like decay. If significant fiber bridging is present, the cohesive law can be broken up into two components, the first of which associated with matrix cracking and the second with fiber bridging. This law takes the name of "bi-linear softening cohesive law" and it is presented in Figure 2.

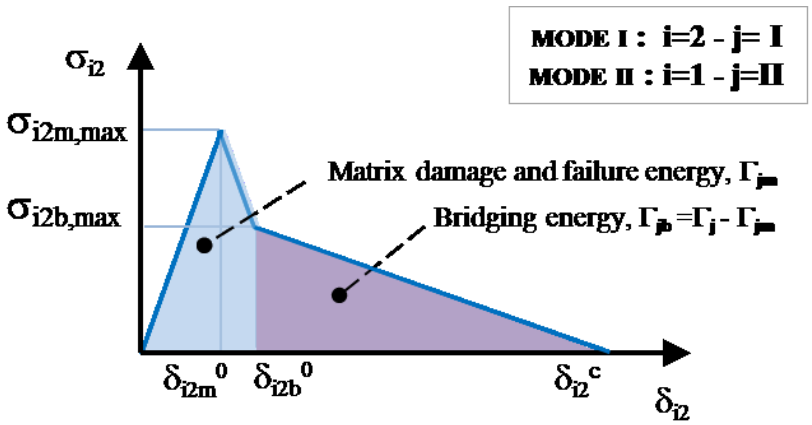

Figure 2.

Subscripts “m” and “b” stand for “matrix” and “bridging” respectively. Superscript “0” indicates the displacement at which the linearity changes, and eventually superscript “c” indicates the critical displacement, at which a complete separation is achieved. This model is based on the idea that the epoxy matrix and the fiber-bridging work as parallel springs: the peak load is reached in correspondence of the matrix cracking ($\sigma_{i2m,max}$, δ_{i2m}^{0}), followed by fiber pull-out beginning at ($\sigma_{i2b,max}$, δ_{i2b}^{0}), until the complete separation (0, δ_{12}^{c}) [31]. This law has been proven [12] to be more appropriate in describing the experimental behaviour than a simple linear damage law such as the one in Figure 1.

The first parameter to be identified is the initial stiffness K_{i2}^{0}, determined by progressively increasing its value until the FE trend coincides with the elastic part of the experimental data. Once the stiffness is established, a value of $\sigma_{i2,max}$ is determined by imposing the cohesive energy $\Gamma_j = G_{jC}$, and then by progressively increasing $\sigma_{i2,max}$ until little if no deviation from linearity is left before the force peak. Finally, the cohesive energy Γ_j is tuned until the post-peak trend has a good convergence. In the case of the bi-linear softening law shown in Figure 2, K_{i2}^{0} and $\sigma_{i2m,max}$ are determined in the same way as for the linear damage law. The value of $\sigma_{i2b,max}$, Γ_{jm} and Γ_j are then identified by trial-and-error process in order to reproduce as closely as possible the data in the post-force peak phase.

The plain weave carbon-epoxy laminate is modelled with the following elastic constants: $E_{11} = E_{22} = 59$ GPa, $E_{33} = 8$ GPa, $G_{13} = 0.8$ GPa, $\nu_{12} = \nu_{23} = 0.261$, $\nu_{13} = 0.062$.

Simulations were carried out using a 2D plane strain finite element model: fully integrated square four-node elements (size 0.25 mm) were used to simulate the cantilevers, while square cohesive elements (size 0.1 mm) were used to simulate the delamination. The force is transmitted via rigid kinematic constraints simulating the fixtures. For ENF specimens, the mesh was refined at the crack tip of the initial delamination, in the region where the crack is expected to propagate, up to 10 mm beyond the half-length of the specimen (in the opposite side of the delamination), due to the fact that it was experimentally found that the crack overcomes the mid-length of the specimen during loading [18]. Figure 3 and Figure 4 show the modelled geometries.

Figure 3.

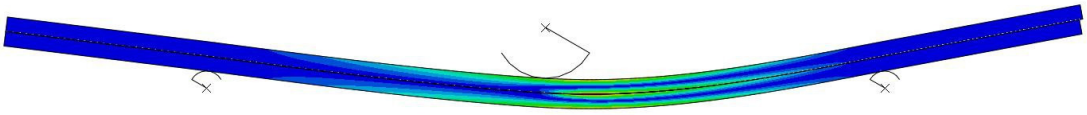

Figure 4.

4. Results

4.1. Mode I

The Mode I fracture behaviour of the virgin material has been initially modelled with the linear damage law represented in Figure 1, for which the area below the traction-separation law is taken equal to the corresponding experimental critical strain energy release rate.

Figure 5 shows the comparison between the experimental result and the numerical solution of a virgin specimen obtained using the linear damage model. Once calibrated, this law fits well to the case of the non-modified interface, where the force/opening presents an initial maximum peak followed by an exponential-like decay.

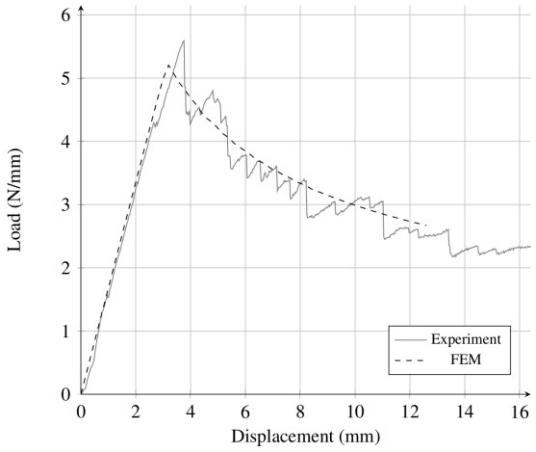

Figure 5.

As found in the literature [32], the linear damage model is rather insensitive to the choice of the critical stress (within some limits: extremely low values of critical stress give poor results in terms of maximum peak force), which here has been chosen high enough to sharpen the force-opening peak as in the experiments. The fracture energy of the cohesive law is obtained varying the value of G_{IC} until a good agreement with the experimental data is reached.

Nanomodified interfaces behave differently due to nanofibers bridging phenomena described in [1], which usually causes a different behaviour during crack propagation. In particular it has been found [12,

18,19] that nanomodified interfaces do not present the classical exponential-like decay, while instead showing a plateau after the peak force, where the load stands before decreasing, as can be seen from the experimental curves in Figure 6. For such cases the triangular law described in Figure 1 is not able to fit the experimental curve, and the bilinear law shown in Figure 2 should be instead used.

Experimental-numerical comparison is shown in Figure 6.

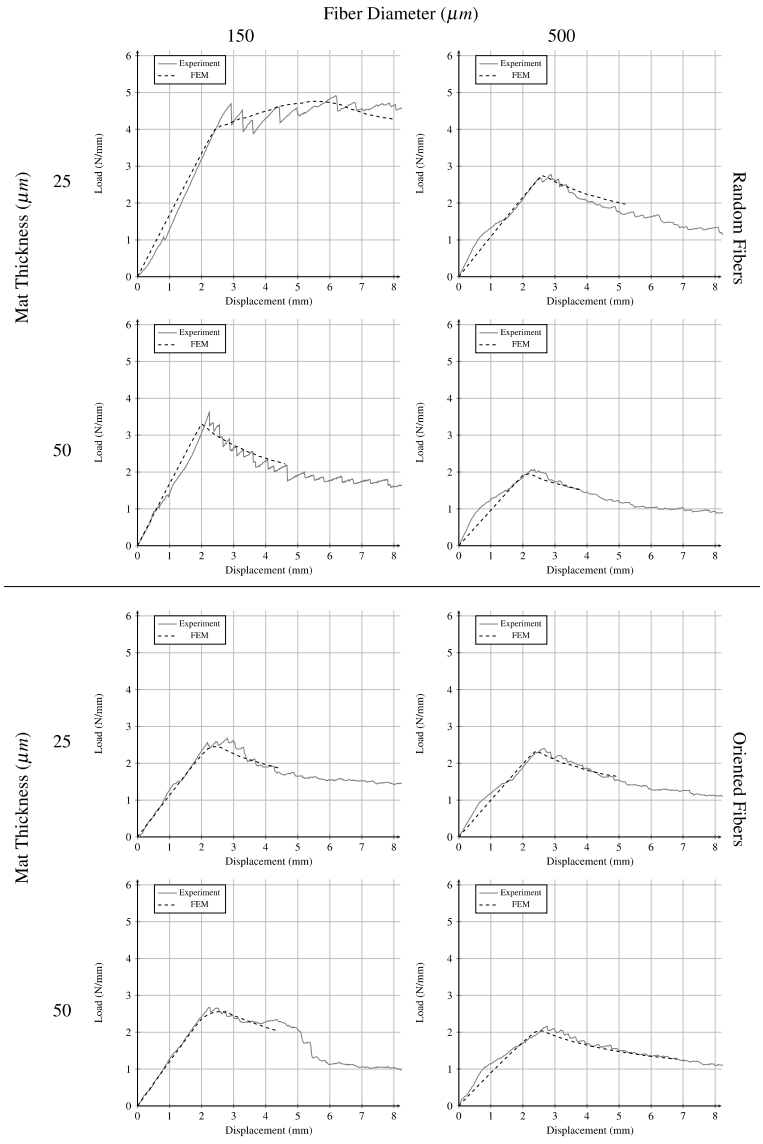

Figure 6.

Model parameters used for the simulations are summarized in Table2.

It can be seen that some tests exhibited a peculiar behaviour in the pre-peak regime, characterized by an initial linear behaviour, followed by a deviation from linearity, then again by a linear segment with lower

slope, until failure. These cases were treated considering only the second linear segment for the simulation of the pre-peak behaviour, implying that a longer crack length was identified in order to match the lower slope of this second linear segment. Model parameters used for the simulations are reported in Table 2.

Table shows that for the 14RB, 14OB and 14OC, a bilinear cohesive law is required: all the "14" configurations (those with 150 nm diameter nanofibers) with exception of the 14RC present a significant fiber bridging phenomena.

4.2. Mode II

In the ENF setup the crack grows rapidly. Experiments showed that, for both virgin and nanomodified specimens, once the crack propagates, the delamination instantaneously overcomes the centreline of the specimen, and consequently the load/displacement graph shows a sharp drop right after the maximum force peak.

The simulation of the virgin specimen was carried out using a linear damage cohesive law, taking the cohesive energy value close to the G_{IIC} determined experimentally.

As mentioned above, the model is rather insensitive to the choice of the critical stress, and then the main parameter is the cohesive energy Γ_{II}. Figure 7 shows two attempts of modelling with different values of Γ_{II}. It is shown that the model cannot simulate well the experimental behavior: in the "Model B" case, the peak load is matched, but the load drop is not deep enough to match the second part of the curve; on the other hand, the "Model A" peak load is underestimated, but the propagation phase is correctly modelled.

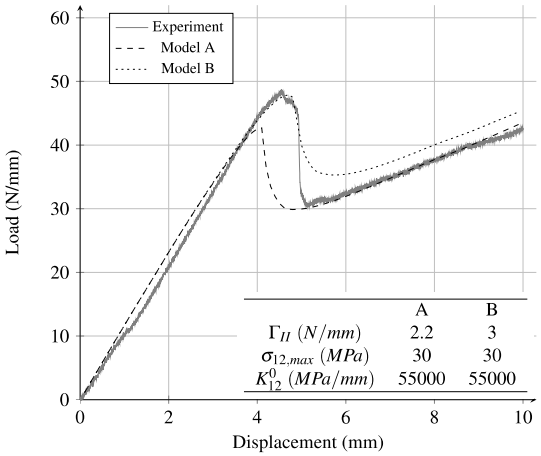

Figure 7.

Therefore, to correctly simulate the behaviour, two different cohesive laws depending on the position along the crack path have been used. The length of the first zone (L_a) is tuned with the experimental results, following these steps:

1. define the parameters to match the maximum load (superscript ' in Figure 8);
2. define the parameters to match the propagation phase (superscript " in Figure 8);
3. assign the parameters obtained with step 1 to those cohesive elements placed after the crack tip for a length of L_a. The parameters obtained with step 2 are given to the remaining elements. Fitting simulations to experiments identifies the value of L_a.

The numerical curve so obtained is plotted in Figure 8, showing a very good agreement with the experimental one. Since no precrack was initiated on the specimens, the first peak load (and therefore the first cohesive law) could be strongly affected by technological issues (position and final edge shape of the Teflon tape), while the second cohesive law is more representative of the material fracture properties. Two cohesive laws are therefore required, since only a constant parameters cohesive law cannot properly simulate the apparent fracture toughness changes along the crack path. This issue could be deeper analysed by modelling the dissipation phenomena at the crack tip (plastic dissipation, fibre bridging), however, this kind of approach is considered to be too demanding to be implemented in an industrial design procedure, and therefore, for this work, out of target.

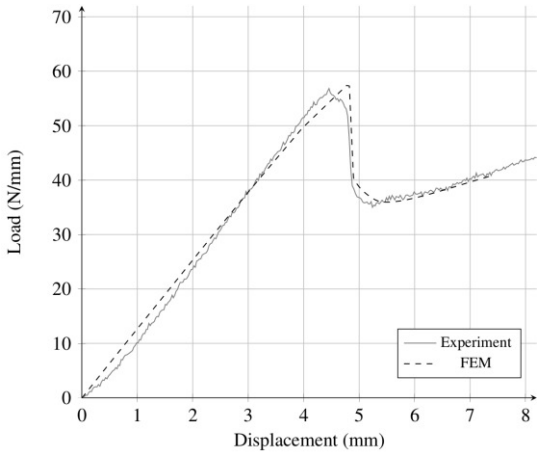

Figure 8.

The same approach in cohesive law identification has been adopted for nanomodified interfaces, and the results are presented in Figure 9.

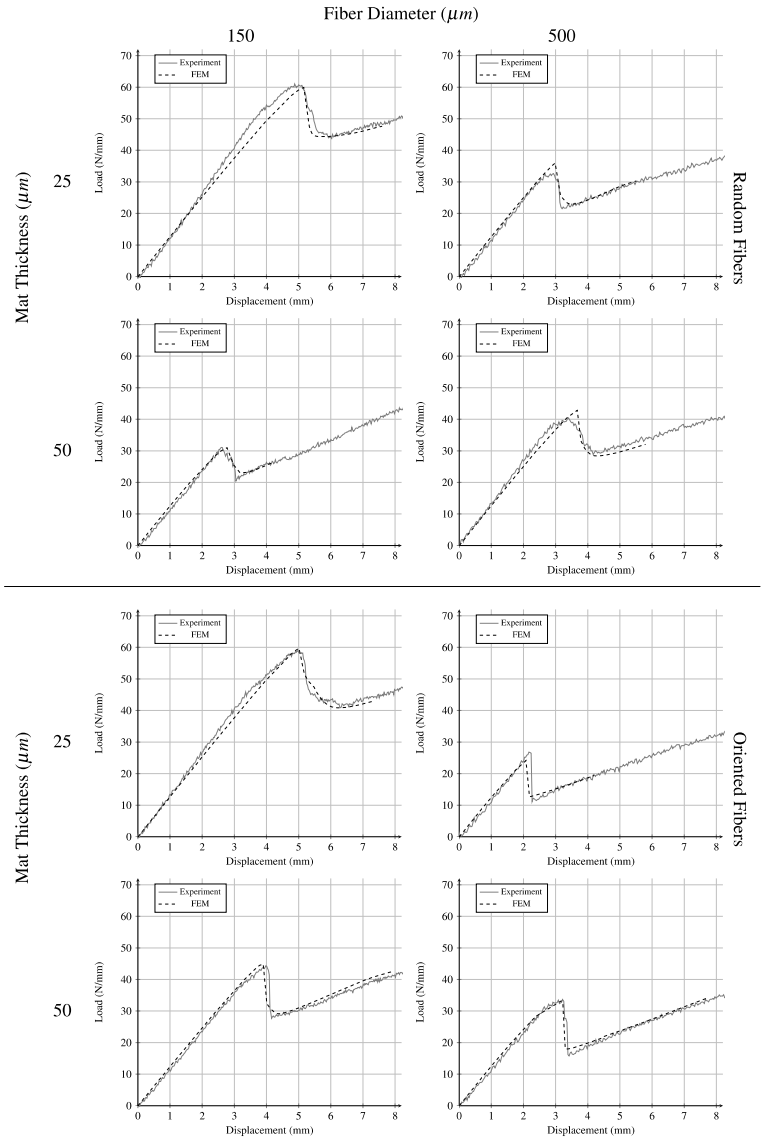

Figure 9.

Model parameters are summarized in Table 3.

5. Discussion

The results shown in the previous section are compared and discussed in order to understand the influence of nanofibers configuration over the cohesive zone parameters, among which, the most significant one is the cohesive energy, representing the delamination fracture toughness.

Considering the mode I tests, therefore looking at Table 2 the following considerations can be drawn:

- 14RB is the only nanomodified configuration showing a cohesive energy higher than virgin material. All the other combinations show a cohesive energy considerably lower;
- the configurations 14RB, 14OB and 14OC require bilinear softening cohesive laws: this could be explained with the presence of significant fiber bridging phenomena, as shown in [1], and reported in Figure 10. However, the amount of energy assigned to the fiber bridging is notably high only in the case of the 14RB specimen;

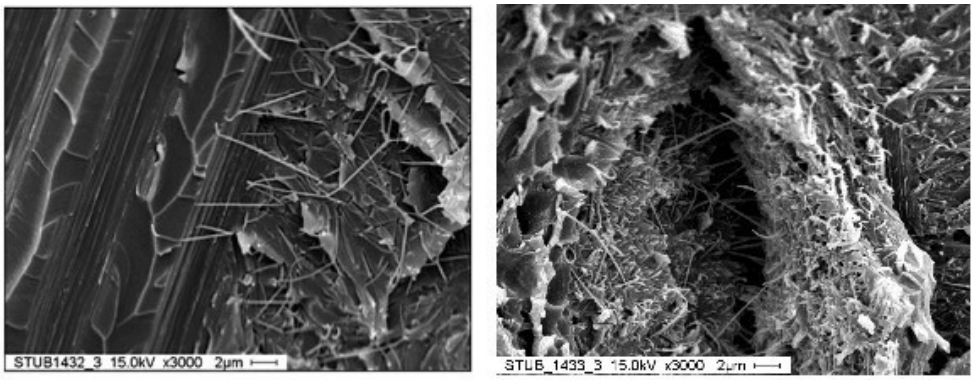

Figure 10.

- Figure 11 reports the values of cohesive energy evaluated for different fiber diameters in the case of different nanofiber orientation and nanolayer thickness.

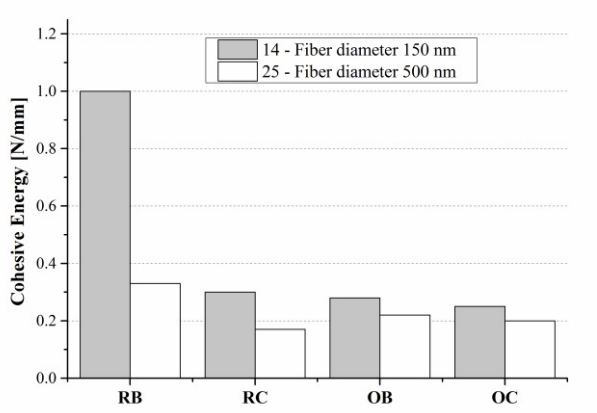

Figure 11.

It can be noticed that the cohesive energy in the case of 150 nm fiber diameter is higher than those of 500 nm fiber for all the configurations, keeping constant the fiber orientation and

nanolayer thickness. This could lead to the statement that the smaller the fiber diameter, the higher the energy absorption capability of the interface;

- in Figure 12 the cohesive energy is evaluated for random and oriented fiber for different values of nanofiber diameter and layer thickness. It appears that, with exception of thicker layer and bigger fiber, random fiber orientation leads to a higher cohesive energy;

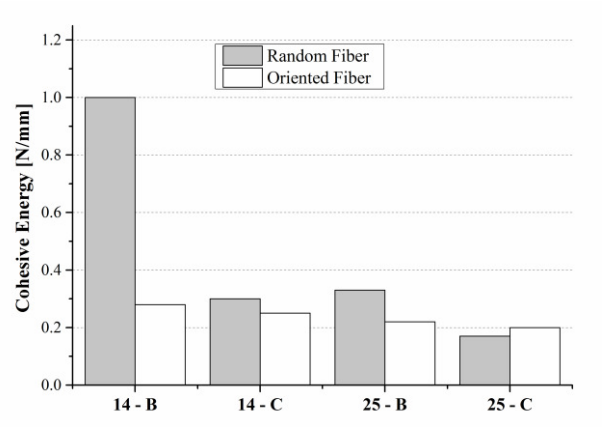

Figure 12.

- Finally Figure 13 compares the cohesive energy for the tested configuration, pointing out the influence of the fiber thickness. It appears that the thinner the fibers, the higher the cohesive energy.

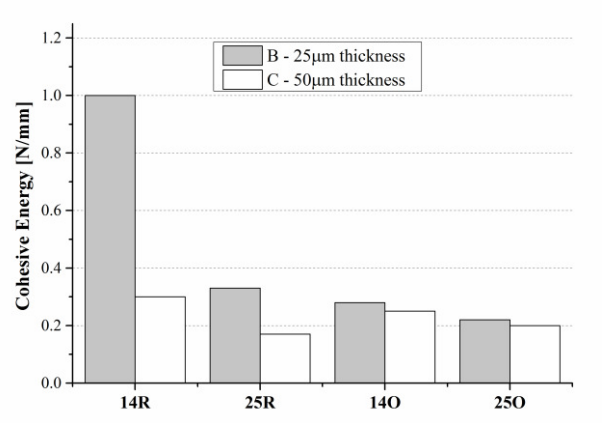

Figure 13.

The cohesive energy is also studied for the mode II tests. Figure14 shows that, with the exception of specimens 25 OB and 25 OC, the cohesive energy of the post-peak cohesive law is higher than that of the pre-peak one. Moreover the specimens 25 OB and 25 OC present the lowest values of the cohesive energy, alike mode I tests.

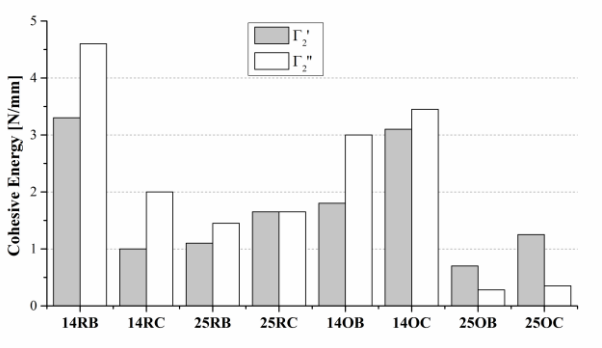

Figure 14.

As previously stated, the pre-peak cohesive law is supposed to be less representative of the steady-state fracture properties than the post-peak one, therefore the latter is considered for the following comparison:

- Figure 15 shows the influence of the fiber diameter for different combination of fiber orientation and layer thickness on Cohesive Energy. It clearly appears that the smaller the fiber diameter, the higher the cohesive energy. This fully confirms the trend already found for the mode I simulations;

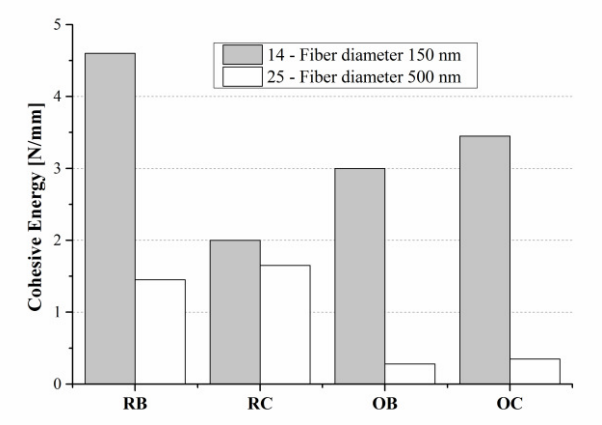

Figure 15.

- Figure 16 shows the influence of fiber orientation over the cohesive energy of mode II tests: a general trend is that random oriented fiber leads to a higher cohesive energy, with the exception of the 14C configuration;

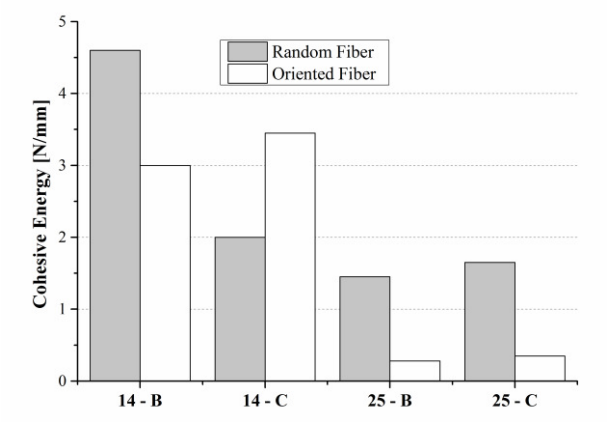

Figure 16.

- Finally, Figure 17 shows the influence of the nanofiber layer thickness, and with exception of the configurations 14R (where the thickness reduction doubles the cohesive energy), it appears that the thicker the layer, the higher the cohesive energy. An opposite trend was found in mode I tests.

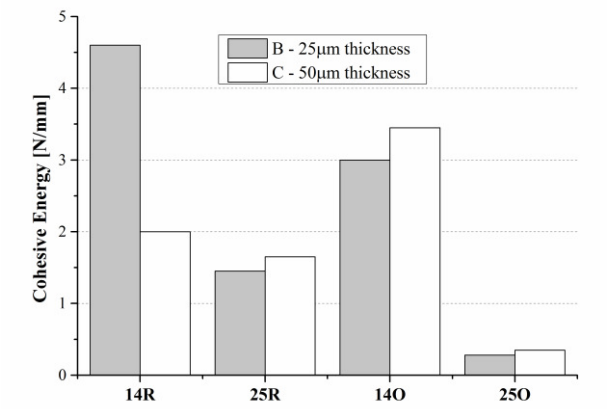

Figure 17.

6. Conclusions

In the present paper, the presence of electrospun nanofibrous mat as interleaving material in composite laminate Mode I and Mode II fracture tests has been numerically simulated using cohesive zone.

For Mode I test simulations, a bilinear damage law came out to be necessary in several cases to match the experimental behaviour of the nanomodified interface, while the virgin material can be represented through a simple linear damage law. The necessity of using a bilinear damage law has been related to the crack bridging and obstacle to crack growth caused by nanofibers. Instead, under Mode II loading virgin

and nanomodified materials behaved similarly until the initiation of fracture, which was matched by a simple linear damage law.

However, in order to match both the starting and steady-state crack propagation phases, a specific procedure for the cohesive parameters identification has been developed, as initial and steady-state cohesive energy values were in general different.

Moreover the influence of the nanomat layer parameters over the cohesive energy is studied in order to link the process parameter to the material strength: the relationship are rather clear concerning the mode I tests, while for the mode II test the trends can be generally understood, hence a more detailed analysis is required, increasing the number of tested specimens and testing pre-cracked specimens.

References

[1] R Palazzetti, I Trendafilova and A Zucchelli. "The self-reinforcing effect of Nylon 6,6 nano-fibres on CFRP composite laminates subjected to low velocity impact." *Composite Structures*,Vol 106, pp.661-671, 2013.

[2] T. Yang, C.H. Wang, J. Zhang, S. He, and A.P. Mouritz. "Toughening and self-healing of epoxy matrix laminates using mendable polymer stitching". *Composites Science and Technology*, Vol. 72, No. 12, pp. 1396–1401, 2012.

[3] E. Fuoss, P.V. Straznicky, and C. Poon. "Effects of stacking sequence on the impact resistance in composite laminates - Part 1: parametric study". *Composite Structures*, Vol. 41, pp. 67–77, 1998.

[4] A.B. Pereira, A.B. de Morais, A.T. Marques, and P.M.S.T. de Castro. "Mode II interlaminar fracture of carbon/epoxy multidirectional laminates". *Composite Science and Technology*, Vol. 64, No. 10-11, pp. 1653–1659, 2004.

[5] W.E. Howard, T. Gossard, R.M. Jones, and M.J. Robert. "Reinforcement of composite laminate free edges with U-shaped caps." *AIAA Paper*, Vol. 1, 1986.

[6] I.K. Partridge and D.D.R. Cartìe. "Delamination resistant laminates by Z-Fiber pinning: Part I manufacture and fracture performance". *Composites Part A: Applied Science and Manufacturing*, Vol. 36, No. 1, pp. 55–64, 2005.

[7] F. Aymerich, F. Dore and P. Priolo. “Prediction of impact-induced delamination in cross-ply composite laminates using cohesive interface elements”. *Composite Science and Technology*, Vol. 68 pp 2383-2390, 2008.

[8] R. Borg. “Simulation of delamination in fiber composites with a discrete cohesive failure model”. *Composites Science and Technology*, Vol. 61, No. 5, pp. 667-677, 2001.

[9] R. Borg. “Modelling of delamination using a discretized cohesive zone and damage formulation”. *Composites Science and Technology*, Vol. 62, No. 10-11, pp. 1299-1314, 2002.

[10] Z. Zou, S.R. Reid, S. Li, and P.D. Soden. “Application of a delamination model to laminated composite structures”. *Composite Structures*, Vol. 56, No. 4, pp 375-389, 2002.

[11] M. Ricotta, M. Quaresimin and R. Talreja. “Mode I strain energy release rate in composite laminates in the presence of voids”. *Composites Science and Technology*, Vol. 68, No. 13, pp. 2616-2623, 2008.

[12] F Moroni, R Palazzetti, A Zucchelli, and A Pirondi. “A numerical investigation on the interlaminar strength of nanomodified composite interfaces” *Composites part B:* Engineering, Vol. 55, pp. 635-641,2013.

[13] N.E. Jansson and R. Larsson. “A damage model for simulation of mixed-mode delamination growth”. Composite Structures, Vol. 53, pp. 1-9, 2001.

[14] A.Turon, P.P. Camanho, J. Costa, and C.G. D’avila. “A damage model for the simulation of delamination in advanced composites under variable-mode loading”. Mechanics of Materials, Vol. 38, No. 11, pp. 1072-1089, 2006.

[15] A.B. Pereira, A.B. de Morais, A.T. Marques and T.P. de Castro. “Mode II interlaminar fracture of carbon/epoxy multidirectional laminates”. Composite Science and Technology, Vol. 64, No. 10-11, pp. 1653-1659, 2004.

[16] S Alessi, M Di Filippo, C Dispenza, ML Focarete, C Gualandi, R Palazzetti, G Pitarresi and A Zucchelli. “Effects of nylon 6,6 nanofibrous mats on thermal properties and delamination behavior of high performance CFRP laminates.” *Polymer Composites*, in press DOI: 10.1002/pc.23035, 2014.

[17] H Saghafi, A Zucchelli, R Palazzetti, G Minak. “The effect of interleaved composite nanofibrous mats on delamination behaviour of polymeric composite materials.” *Composite Structure*, Vol. 109, pp. 41-47, 2014.

[18] R Palazzetti, XT and A Zucchelli. "Influence of geometrical features of electrospun Nylon 6,6 interleave on the CFRP laminates mechanical properties". *Polymer Composites*, Vol. 35, No. 1, pp. 137-150, 2014.

[19] R. Palazzetti, A. Zucchelli, C. Gualandi, M.L. Focarete, L. Donati, G. Minak and S. Ramakrishna. "Influence of electrospun Nylon 6.6 nanofibrous mats on the interlaminar properties of Gr-Epoxy composite laminates". *Composite Structures*; Vol. 94, No. 2, pp 571-579, 2012.

[20] A. Zucchelli, M.L. Focarete, C. Gualandi, and S. Ramakrishna. "Electrospun nanofibers for enhancing structural performance of composite materials". *Polymers Advanced Technologies*, Vol. 22, No. 3, pp. 339–349, 2011.

[21] D.S. Dugdale. "Yielding of steel sheets containing slits". *Journal of Mechanics, Physics and Solids*, Vol. 8, pp.100–104, 1960.

[22] G.I. Barenblatt, "The mathematical theory of equilibrium cracks in brittle fracture". *Advanced Applied Mechanics*, Vol. 7, pp. 55-129, 1962.

[23] G.T. Camacho and M. Ortiz. "Computational modelling of impact damage in brittle materials". *International Journal of Solid Structures*, Vol. 33, pp. 2899–2938, 1996.

[24] V. Tvergaard, and J.W. Hutchinson. "The relation between crack growth resistance and fracture process parameters in elastic–plastic solids". *Journal of Mechanics Physics and Solids* Vol. 40, pp. 1377–1397, 1992.

[25] X.P. Xu and A. Needleman. "Void nucleation by inclusions debonding in a crystal matrix". *Modeling and Simulation in Materieal Science and Engineering* Vol. 1, pp. 111–132, 1993.

[26] G. Mancusi and F Ascione. Failure Criteria for FRP Adhesive Lap Joints: A Comparative Analysis. *Mechanics of Advanced Materials And Structures*. Vol. 17. Pag.157-164 ISSN:1537-6494

[27] F. Ascione. Ultimate behaviour of adhesively bonded FRP lap joints. *Composites. Part b, Engineering*. Vol. 40. Pag.107-115 ISSN:1359-8368

[28] M.F.S.F. de Moura, J.A.G. Chousal, Cohesive and continuum damage models applied to fracture characterization of bonded joints, *International Journal of Mechanical Sciences* 48 (2006) 493–503

[29] S. Li, M.D. Thouless, A.M. Waas, J.A. Schroeder and P.D. Zavattieri. "Use of mode-I cohesive-zone models to describe the fracture of an adhesively-bonded polymer–matrix composite". *Journal of Composite Science and Technology*, Vol. 65, pp. 537–549, 2005.

[30] A. Turon, C. Davila, P. Camanho and J. Costa. "An engineering solution for mesh size effects in the simulation of delamination using cohesive zone models". *Engineering Fracture Mechanics*, Vol. 74, No. 10, pp. 1665-1682, 2007.

[31] Li S, Thouless MD, Waas AM, Schroeder JA, Zavattieri PD. Use of a cohesive-zone model to analyze the fracture of a fiber-reinforced polymer–matrix composite. *Composite Science and Technology*, Vol. 65, pp. 537-549, 2011.

[32] Xie D, Waas A. Discrete cohesive zone model for mixed-mode fracture using finite element analysis. *Engineering Fracture Mechanics*; Vol. 73(13), pp. 1783-1796, 2006.

Figure Captions

1. Linear damage cohesive law.
2. Bi-linear softening traction–separation law used to describe fracture of layers with fiber bridging.
3. DCB model
4. ENF model.
5. Comparison between experiment and cohesive zone model in the case of virgin laminate.
6. Experimental (continue lines) and numerical (dashed lines) results for Mod I tests.
7. Result of ENF (virgin material) simulation obtained using a triangular shape cohesive law.
8. Result of ENF (virgin material) simulations obtained using two triangular shape cohesive laws.
9. Experimental (continue lines) and numerical (dashed lines) results Mod II tests.
10. SEM pictures of nanofiber bridging after crack propagation
11. Influence of the fiber diameter for different fiber orientation and layer thickness.
12. Influence of the fiber orientation for different fiber diameter and layer thickness.
13. Influence of the layer thickness different fiber diameter and fiber orientation.
14. Cohesive energies identified for Mode II loading
15. Influence of the fiber diameter for different fiber orientation and layer thickness.
16. Influence of the fiber orientation for different fiber diameter and layer thickness.
17. Influence of the layer thickness different fiber diameter and fiber orientation.

Tables

Table 1. Nanofiber configurations.

Nanofiber Diameter	Nanofiber Orientation	Nanolayer Thickness	Code
150 nm (14)	Random (R)	25 μm (B)	14RB
		50 μm (C)	14RC
	Oriented (O)	25 μm (B)	14OB
		50 μm (C)	14OC
500 nm (25)	Random (R)	25 μm (B)	25RB
		50 μm (C)	25RC
	Oriented (O)	25 μm (B)	25OB
		50 μm (C)	25OC

Table 2. Cohesive zone parameters identified for Mode I simulations.

DCB	Cohesive Zone Parameters				
Code	Γ_I (N/mm)	$\sigma_{22m,max}$ (MPa)	K^0_{22} (MPa/mm)	$\sigma_{22b,max}$ (MPa)	Γ_{Ib}' (MPa/mm)
Virgin	0.75	60	55000	/	/
14RB	1	48	55000	1	0.45
14RC	0.3	38	55000	/	/
25RB	0.33	25	55000	/	/
25RC	0.17	40	55000	/	/
14OB	0.28	23	55000	1	0.22
14OC	0.25	20	55000	1	0.22
25OB	0.22	30	55000	/	/
25OC	0.2	8	55000	/	/

Table 3. Cohesive zone parameters identified for Mode II loading.

	Cohesive Zone Parameters						
Code	**Γ_{II}' (N/mm)**	**σ_{12max}' (MPa)**	**K^0_{12}' (MPa/mm)**	**Γ_{II}'' (N/mm)**	**σ_{12max}'' (MPa)**	**K^0_{12}'' (MPa/mm)**	**L_a (mm)**
Virgin	3	30	55000	2.2	30	55000	10
14RB	3.3	40	55000	4.6	51	55000	20
14RC	1	17.5	55000	2	35	55000	25
25RB	1.1	30	55000	1.45	30	55000	25
25RC	1.65	30	55000	/	/	/	/
14OB	1.8	35	55000	3	48	55000	25
14OC	3.1	45	55000	3.45	48	55000	10
25OB	0.7	14	55000	0.28	7	55000	10
25OC	1.25	17	55000	0.35	8	55000	20